

**Structural and dynamical characterization
of non-muscle myosin heavy chain II-B
in epithelial Madin-Darby canine kidney II cells**

Bachelor thesis in Biochemistry

Natalie Zwing

geboren am 03.02.1990

in

Starnberg

Bachelorarbeit beim Prüfungsausschuss eingereicht am 04.02.2013

Erklärung

Ich versichere, dass ich meine Bachelorarbeit am

Max Planck Institute of Biochemistry
in der Arbeitsgruppe Cellular Dynamics and Cell Patterning,
geleitet von Herrn Dr. Roland Wedlich-Söldner

unter der Anregung und Anleitung von

Dr. Roland Wedlich-Söldner und Christoph Klingner

Selbstständig durchgeführt und keine anderen als die angegebenen Hilfsmittel und Quellen
benutzt habe.

München, _____

Unterschrift

Erstgutachter: _____

Zweitgutachter: _____

Abstract

Non-muscle myosin II, an actin-binding motor protein, plays an essential role in actin cytoskeleton organization and cellular motility. Actin filaments, key cytoskeletal elements mostly located close to the cell cortex, can generate in combination with myosin proteins protrusive or contractile forces. Members of the Wedlich-Söldner group recently identified an isotropic cortical myosin network at the apical side of non-polarized MDCK II epithelial cells, containing non-muscle heavy chain II-A (NMHCII-A) and myosin regulatory light chain (MRLC). During our studies, we investigated the characteristics of non-muscle myosin II-B (NMHCII-B), conducting methods in molecular biology, cell culture and live cell imaging.

In comparison to NMHCII-A, the myosin isoform II B shows the same isotropic network at the apical side and stress fiber structures at the basal side of MDCK II cells. Furthermore, NMHCII-B proteins rearrange highly dynamics within the cell cortex. Additionally, we identified a global oscillatory behavior using autocorrelation analysis methods, marked by states of low and high rearrangement activity. These features give important insights into localization and dynamics of the non-muscle myosin II-B motor protein in epithelial cells.

Table of contents

Erklärung	II
Abstract	III
1 Introduction	1
2 Material and Methods	3
2.1 Material	3
2.1.1 Chemicals	3
2.1.2 Plasmid constructs	3
2.1.3 Enzymes and Enzyme buffers	3
2.1.4 Cell types.....	4
2.1.5 Media.....	4
2.1.6 Buffers and Solutions	5
2.1.7 Primers	5
2.1.8 Devices and Commercial kits.....	5
2.1.9 Equipment	6
2.1.10 Software.....	6
2.2 Methods.....	7
2.2.1 Molecular Biology.....	7
2.2.1.1 Cloning Strategy.....	7
2.2.1.2 Agarose gel electrophoresis.....	7
2.2.1.3 Elution of DNA fragments and ligation	8
2.2.1.4 Transformation of E. coli cells	8
2.2.1.5 Restriction digest.....	9
2.2.1.6 Sequencing	9
2.2.2 Cell culture	10
2.2.2.1 Preparation of cells – Defrosting, Splitting, Counting	10
2.2.2.2 Transfection procedures – establishing stable cell lines/transient transfection	10
2.2.3 Microscopy – Live cell imaging.....	12
2.2.4 Temporal autocorrelation (Pearson).....	13

3 Results	14
3.1 Molecular Biology.....	14
3.1.1 Cloning Strategies	14
3.1.2 Ligation procedure	19
3.1.3 Restriction digests	19
3.1.4 Sequencing	25
3.2 Cell culture	25
3.3 Characterization.....	26
3.3.1 Structure of NMHCII-B	26
3.3.2 Dynamical behavior	29
4 Discussion	34
4.1 Molecular Biology.....	34
4.2 Cell culture	34
4.3 Live cell imaging.....	34
5 References	37
6 Acknowledgements.....	38

1 Introduction

Myosin II is a major motor protein, which is critical for the cell to contract and to move based on its contractile interaction with actin filaments, helical structures of polymerized globular actin strands. The hexameric protein myosin complex consists of a pair of heavy chains (MHCII), a pair of essential light chains (MELC), stabilizing the heavy chain structure, and a pair of regulatory light chains (MRLC), regulating the myosin II ATPase activity. An N-terminal conserved motor domain containing an actin binding site drives the myosin along actin filaments. Non-conserved α -helical coiled-coil C-terminal domains, terminating in a short rod non-helical tail, MHCII proteins form bipolar minifilaments by self-association. Producing tension on actin by polar movement on antiparallel filaments, the actin-dependent myosin II motors convert chemical energy into mechanical force, provided by ATP hydrolysis. The complex composing of myosin II and actin is called actomyosin [1,2].

In this thesis I outline the localization and dynamics of the non-muscle myosin II-B (NMHCII-B) motor protein in epithelial cells. As common standard model organism we used Madin-Darby canine kidney (MDCK) II cells for our experiments, exhibiting a number of myosin II dependent structures, such as stress fiber formation, cell-adhesion and cell junctions [3]. NMHCII-B belongs to one of the three isoforms of the non-muscle myosin II family along with NMHCII-A and NMHCII-C [1,2]. During a current project in the group of Roland Wedlich-Söldner an isotropic cortical myosin network at the apical side of MDCKII cells has been identified. The network contains NMHCII-A and MRLC and shows highly dynamic behavior. Computer based image analysis revealed oscillating periods of myosin activity. Previous studies on myosins in MDCK II cells depict the presence of NMHCII-A and NMHCII-B, but not NMHCII-C. However, little is known about the function of NMHCII-B [3]. Although NMHCII-A and NMHCII-B are partly redundant, recent studies in normal mouse mammary gland and breast epithelial cell lines show unique roles of the respective isoforms [4]. Other studies on the contrary reveal that no isoform can be replaced by another in many biological contexts. Kinetic properties show differences in actin-activated Mg^{2+} -ATPase activity (higher for MHCII-A), duty ratio (higher for MHCII-B) and in releasing time of ADP (longer for MHCII-B) [5]. It is therefore of high interest if NMHCII-B in comparison to NMHCII-A localizes to the new cortical myosin network at the apical side of non-polarized MDCK II cells and if it contributes to oscillatory behavior.

To address this question our experimental work is divided into four parts. First, we generated expression constructs for GFP-tagged NMHCII-B (pEFIRES_eGFP_NMHCII-B_puro and NHMCII-B_GFP_Hyg) using standard molecular biology approaches. Second, we established cell lines by transiently expressing the respective plasmids by lipofection. Different fluorophores additionally allowed to express NMHCII-B plasmids with NMRLC plasmids in one cell line. All cell lines were checked in detail for possible overexpression effects. Third, we investigated the cellular localization of NMHC-II-B and its dynamics by using high resolution fluorescence microscopy. Fourth, the obtained data was analyzed by established matlab-based filters and algorithms. Lastly, the results of this thesis led to a better understanding of the role of NMHC-II-B in cortical acto-myosin networks of epithelial cells.

2 Material and Methods

2.1 Material

2.1.1 Chemicals

Table 1: Chemicals used for experiments.

Chemical	Supplier	Chemical	Supplier
Agar	Becton Dickinson	Ethidium bromid 1 %	Carl Roth
Agarose	Invitrogen	Glycerin	Carl Roth
Ampicillin	Carl Roth	Hygromycin	Roche
ddH ₂ O	Cutsom made	Lipofectamine	Invitrogen
DMSO	Sigma-Aldrich	Puromycin	Life Technologies
Ethanol 70 %	Sigma-Aldrich	Trypsin	Life Technologies

2.1.2 Plasmid constructs

The plasmid constructs were available in the plasmid library of Roland Wedlich-Söldner group for cloning strategy and transfection procedures.

Table 2: Plasmid constructs used for cloning strategies and transfection procedures.

Plasmid
RWM136_pEFIRES_P_empty
RWM140_CMV-GFP-NMHCII-B
RWM65_pAcGFP1-Hyg-Cm_empty
RWM142_pEGFP-N1-Lifeact-Hyg

2.1.3 Enzymes and Enzyme buffers

Table 3: Enzyme buffers used for molecular biology.

Enzyme buffer	Supplier
NEBuffer	New England BioLabs
T4 Buffer	New England BioLabs

Table 4: Enzymes used for molecular biology.

Enzyme	Supplier
AgeI	New England BioLabs
ClaI	New England BioLabs
EagI-HF	New England BioLabs
EcoRI	New England BioLabs
MfeI-HF	New England BioLabs
NheI-HF	New England BioLabs
NotI-HF	New England BioLabs
T4 DNA ligase	New England BioLabs
XhoI	New England BioLabs

2.1.4 Cell types

Table 5: Cell types used for experiments.

Cell type	Abbreviation
Cervical cancer cells of Henrietta Lacks	HeLa
Escherichia coli	E. coli
Madin-Darby canine kidney II	MDCK II

2.1.5 Media

Table 6: Media used for experiments.

Medium	Supplier
DMEM + GlutaMax™	Life Technologies
Fetal bovine serum (FBS)	Life Technologies
Optimem	Life Technologies
YT-Medium	-

2.1.6 Buffers and Solutions

Table 7: Buffers and Solutions used for experiments.

Buffer/Solution
6x loading dye
10x TBE-Buffer
GeneRuler™ DNA Ladder Mix

2.1.7 Primers

Table 8: Primers used for sequencing.

Name	Alias	Sequence (5' → 3')
5'-NMHCII-B-2	RWS1449	CGGGACAGCAAGACAAAG
5'-NMHCII-B-10	RWS1457	GCTATTTTCAGTGAGCAAAGCTG
3'EGFP-seq	RWS927	CCAGCTCGACCAGGATGG
IRES-3'sec	RWS2137	GAGGAACTGCTTCCTTCACG

2.1.8 Devices and Commercial kits

Table 9: Devices and commercial kits used for experiments.

Products	Supplier
Falcons 10 ml; 50 ml	Sarstedt
Lens paper	Schütt Labortechnik
Microscope dishes – cells in focus	Ibidi
Pasteur pipettes	Brand
Pipette tips	Peske
Pipettes 5 ml; 10 ml; 25 ml	Sarstedt
Plasmid Mini Kit I	Omega Bio-tek
Tissue Culture Dishes	Sarstedt
Tissue Culture Flasks	Becton Dickinson Labware
Tubes 1,5 ml; 2,0 ml	Eppendorf
Well Cell Culture Cluster (24; 12; 6)	Costar
Wizard® SV Gel and PCR Clean-Up System	Promega

2.1.9 Equipment

Table 10: Equipment used for experiments.

Instrument	Supplier
AQUALine AL25	LAUDA
Centrifuge Heraeus Pico 17	Thermo Electron Corporation
Freezer -20 °C	Beko
Freezer -50 °C	New Brunswick Scientific
Hera Safe hood	Thermo Electron Corporation
Heraeus Multicentrifuge 3S	Thermo Electron Corporation
Incubator Hera cell 240	Thermo Electron Corporation
Incubator Heraeus Function Line	Thermo Electron Corporation
Incubator shaker innova™ 4230	New Brunswick Scientific
NanoDrop 2000c	Thermo Scientific
Neubauer chamber	Marienfeld Germany
Pipetus	Hirschmann Laborgeräte
Refrigerator 2 - 8 °C	Liebherr
Transilluminator®, dark shaker	Clare Chemical Research
Vacu Hand Control	Vacuubrand
Vortex-shaker	VWR International

2.1.10 Software

Table 11: Software used for experiments.

Software	Function	Supplier
A plasmid Editor (ApE) v2.0.45	Plasmid editing	M. Wayne Davis
Origin® Pro 9.0	Data plotting	OriginLab Corporation
Live Acquisition	Microscope controlling	Till Photonics
Chromas Lite	Sequencing analysis	Freeware

2.2 Methods

2.2.1 Molecular Biology

2.2.1.1 Cloning Strategy

To amplify the NMHCII-B gene sequence, we used two different DNA cloning strategies. Following a cut and paste procedure, a backbone construct and a construct with the insert sequence were available in the plasmid library of Wedlich-Söldner group respectively. Specific restriction enzymes isolated the NMHCII-B sequence and opened the backbone, conducting two separated digest preparations (table 12).

Table 12: Digest preparation for insert and backbone construct.

Insert		Backbone	
5 µl	DNA	3 µl	DNA
5 µl	10x BSA	3 µl	10x BSA
5 µl	NEbuffer	3 µl	NEbuffer
2 µl	enzyme 1	0,5 µl	enzyme 1
2 µl	enzyme 2	0,5 µl	enzyme 2
31 µl	ddH ₂ O	20 µl	ddH ₂ O
50 µl	total	30 µl	total

There are four standard NEbuffers, which conditions are selective for each enzyme activity. We only used NEbuffer 4, as it worked for all chosen restriction enzymes for our cloning strategies. After mixing the components, the digestions were incubated at 37 °C for 2 h.

2.2.1.2 Agarose gel electrophoresis

Using agarose gel electrophoresis, it was possible to extract the insert and the backbone fragments. Secondly, this method was used to proof correct synthesized new constructs by conducting restriction digests.

Table 13: Components for an 0,8 % and 1 % agarose gel.

0,8 % agarose gel		1 % agarose gel	
0,4 g	agarose powder	0,5 g	agarose powder
50 ml	1x TBE buffer	50 ml	1x TBE buffer
6 µl	ethidium bromide	6 µl	ethidium bromide

Loading DNA samples, 6 µl 6x loading dye was added respectively. A GeneRuler™ DNA Ladder Mix was additionally loaded, determining the sizes of the DNA fragments. All gels were running at 115 V for 35 min. By means of a transilluminator the DNA fragments labeled with ethidium bromide were observable.

2.2.1.3 Elution of DNA fragments and ligation

For subsequent experimental steps, the identified fragments of the backbone and the insert were cut out of the gel (black holes Fig. 1 and 2). Afterwards the DNA was eluted, using the Wizard SV Gel and PCR Clean-Up System of Promega.

Using 1 µl of the enzyme T4 DNA ligase, the digested DNA fragments were ligated in a specific ratio between the backbone and the insert fragments dependent on the different lengths. The backbone input basically accounted 30 µg. Additionally, 2 µl T4 buffer was added and the mixture was filled up to 20 µl total with ddH₂O. The separated reaction mixtures were incubated at room temperature for 2 h and subsequently transformed in *E. coli* cells.

2.2.1.4 Transformation of *E. coli* cells

To amplify the new plasmid constructs, competent *E. coli* cells were used for transformation of the DNA. Therefore, the bacterial cell line, stored at -80 °C, was firstly kept on ice, defrosting them slowly, for 10 min. 50 µl *E. coli* cells were added to a mixture of 5 µl ligation DNA and 5 µl ddH₂O and kept on ice for 30 min again. The aliquot was heat shocked at 42 °C for 2 min, calmed down at 4 °C for 2 min and 150 µl YT medium was added. After storing at 37 °C for 20 min, bacteria cells were plated on ampicillin-resistance medium and incubated at 37 °C overnight.

For amplification of plasmid constructs, several grown colonies were picked and injected in 3 ml liquid YT-medium containing ampicillin. Lastly, the DNA plasmid was isolated out of the bacteria cells, using the Plasmid Mini Kit I of Omega and its respective protocol.

2.2.1.5 Restriction digest

All obtained plasmids were subsequently analyzed using restriction digests to check for accurate cloning. In table 14 a general preparation protocol is listed. Besides all new construct samples, the backbone, the origin plasmid with the insert sequence and the uncut version of one DNA sample were tested respectively.

Table 14: Restriction digest.

1 μ l	DNA
2 μ l	10x BSA
2 μ l	NEbuffer 4
0.5 μ l	enzyme
14,5 μ l	ddH ₂ O
<hr/>	
20 μ l	total

2.2.1.6 Sequencing

To verify a correct insertion of NMHCII-B sequence and to test the cutting sites, we ordered a sequencing of the Biochemistry Core Facility. They used Modified Sanger dideoxy terminator cycle sequencing chemistry. The primer was diluted in ddH₂O in a 1:10 ratio.

Table 15: Sequencing preparation for Core Facility.

1 μ l	primer
2 μ l	plasmid DNA
4,5 μ l	ddH ₂ O
<hr/>	
7,5 μ l	total

For further analysis of the sequencing, we used ApE & Chromas Lite Software.

2.2.2 Cell culture

2.2.2.1 Preparation of cells – Defrosting, Splitting, Counting

The wildtype (WT) cells of Madin-Darby canine kidney (MDCK) are usually stored at -80 °C in 90 % fetal bovine serum (FBS), additionally containing 10 % Dimethyl sulfoxid (DMSO) as antifreezing compound. As growth medium for these epithelial cells served DMEM + GlutaMax™, with additive 10 % FBS. Subsequently, this composition will be abbreviated only as DMEM. Furthermore, all components had to be warmed up to 37 °C and disinfected before usage under the cell culture hood.

Defrosting the mammalian cells, the aliquot was kept in a 37 °C water bath for 2 min. To get rid of DMSO, the solved cells were centrifuged at 2000 rpm for 2 min in a falcon tube with 1 ml of DMEM medium. Afterwards, the supernatant was discarded with a vacuum pump, the cell pellet was resolved with 1 ml DMEM and the whole aliquot was transferred to a flask, filled with 5 ml DMEM. For adherent growing, the wildtype cells were incubated at 37 °C.

To avoid cell death, owing to confluency or decreasing nutrients, the MDCK culture required a splitting procedure every 2 to 3 days. The medium was discarded, the cells washed one time with 3 ml 1x Phosphate buffered saline (PBS) and treated with 3 ml 1x trypsin for 15 min at 37 °C, to detach MDCK WT cells. After complete detachment of cells, the procedure was stopped by adding 3 ml growth medium. 1 ml of the cells were then transferred to a new flask with new 5 ml DMEM and stored at 37 °C again. For subsequent transfection of plasmid DNA, 10.000 to 100.000 MDCK cells were plated in 12 well-plates. For cell counting we used a Neubauer chamber.

2.2.2.2 Transfection procedures – establishing stable cell lines/transient transfection

The transfection procedure was conducted as presented in the following schematic diagram (Fig. 1). Depending on DNA concentrations, measured with NanoDrop2000c, an input of 1 to 2 µg DNA was calculated, respectively.

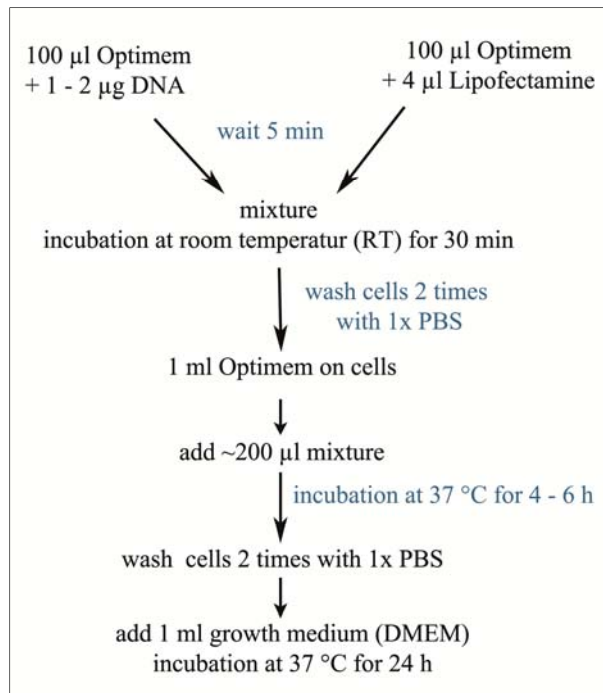


Figure 1: Description of a general transfection procedure.

For establishing stable cell lines the DMEM was discarded 24 h after transfection procedure, the cells washed with 1 ml 1x PBS and treated with 0,5 ml Trypsin for 15 min. By adding 0,5 ml DMEM the detachment procedure was stopped. 1 ml of the cell solution was then transferred from wells to separate petri dishes, filled with 9 ml DMEM and incubated at 37 °C for 24 h. For cell selection containing the new construct, a respective selection marker was added after incubation. Medium and respective antibiotic were changed every 48 h. After isolating cell clones and separate growing on well plates, the cells were transferred on microscope dishes for live cell imaging.

A transient transfection followed the same protocol as shown in Fig. 1. The distinction in producing transient cells was to trypsinate transfected MDCKs for transfer in small microscope dishes already 24 h after transfection or to plate cells directly in microscope dishes for transfection procedure.

2.2.3 Microscopy – Live cell imaging

To control cell growing and to follow detachment procedures during transfection, we visualized cells with a light microscope. For further examining, we used a standard Wide Field Fluorescence Microscope to firstly control a fluorescence expression within the transfected cells.

Detailed live cell imaging was performed on an iMIC stand (Till Photonics) with an Olympus x100 1.45 NA objective. For GFP extinction a DPSS laser (75 mW) at 488 nm (Coherent Sapphire) was selected through an acousto-optical tunable filter [6]. Image acquisition was performed with an Imago-Qe SensiCam CCD camera controlled by the Live Acquisition (Till Photonics) software. Double color images were obtained by using a tunable monochromator and respective filter sets. An examination of raw imaging data (Fig. 2a) was conducted with Fiji software. For subsequent analysis images were filtered, using Matlab algorithms. The filtering system consisted of a Block Matching 3D Filtering (BM3D) followed by a local Rolling Ball (LRB) Filter Process. For filtering elongated structures the BM3D algorithm was important, to estimate the original, noise-free image (Fig. 2b). Using Fiji, a 3D information image (Fig. 3) was established by maximal projection of various planes and subsequent color coding different cell height levels.

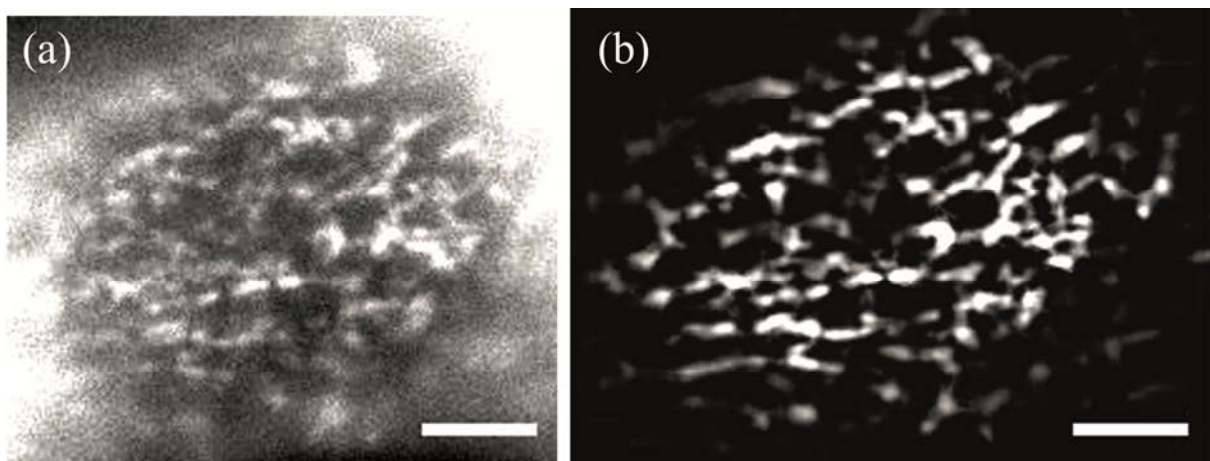


Figure 2: Live cell imaging and subsequent filtering. (a) Raw data of an apical NMHCII-B structure in MDCK cells and (b) filtered data of the same image; Scale bar: 3 μm .

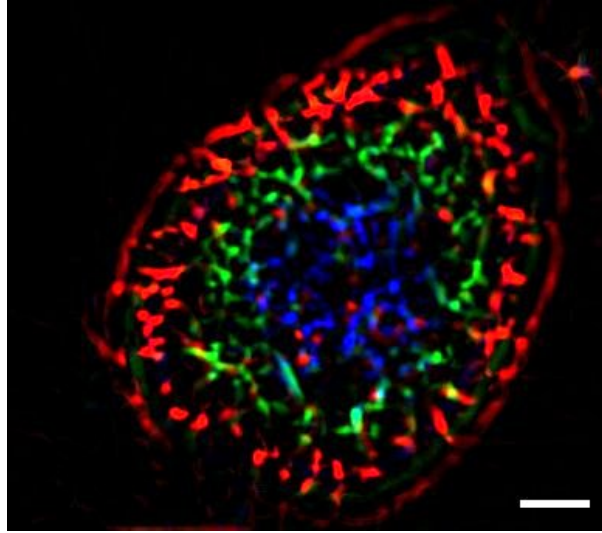


Figure 3: Image with 3D information of the apical side of a MDCK cell transfected with NMHCII-B. Scale bar: 3 μm . Due to overexpression artifacts the red colored level shows cytosolic myosin II aggregates transported in vesicles.

2.2.4 Temporal autocorrelation (Pearson)

To quantify dynamical rearrangement of NMHCII-B, we measured the similarity of filtered image frames from time-lapse movies by calculating the Pearson correlation coefficient r using Matlab Software. For two images X and Y the Pearson correlation coefficient r is:

$$r(X, Y) = \frac{\sum_{i=1}^n (X_i - \langle X_i \rangle)(Y_i - \langle Y_i \rangle)}{\sqrt{\sum_{i=1}^n (X_i - \langle X_i \rangle)^2} \sqrt{\sum_{i=1}^n (Y_i - \langle Y_i \rangle)^2}}$$

The subscript i denoted the i^{th} pixel of the image and brackets showed the average over all pixels in the image. A movie consisted of frames, which were established after every 5 seconds. Using the first frame X^0 as reference, r was calculated by comparing X^0 with all following frames X^t [7]. By plotting the Pearson correlation coefficient r against time t with ‘Origin Pro 9.0 Software’, an experimental decay of r was observable.

Moreover, we performed additional temporal autocorrelation analysis by changing the reference frame of Pearson correlation following the order X^0, X^1, \dots . For every reference frame we subsequently calculated the Pearson correlation coefficients as well as fitted the respective correlation time τ . This analysis method allowed for the examination of the temporal change of reorganization speeds within the network structures.

3 Results

3.1 Molecular Biology

3.1.1 Cloning Strategies

To construct a NMHCII-B puromycin plasmid **pEFIRES_eGFP_NMHCII-B_puro**, we used a three fragment ligation cloning strategy, including the backbone and the non-muscle myosin heavy chain II B sequence as the insert. For this purpose two constructs from the plasmid library of Wedlich-Söldner group were available: RWM136_pEFIRES_P_empty construct (Fig. 4a) serving as the new backbone and RWM140_CMV-GFP-NMHCII-B construct (Fig. 4b) with the NMHCII-B insert sequence. Featuring a geneticin-resistance gene as a rather weak selection marker, the RWM140 plasmid could not be used to establish stable cell lines.

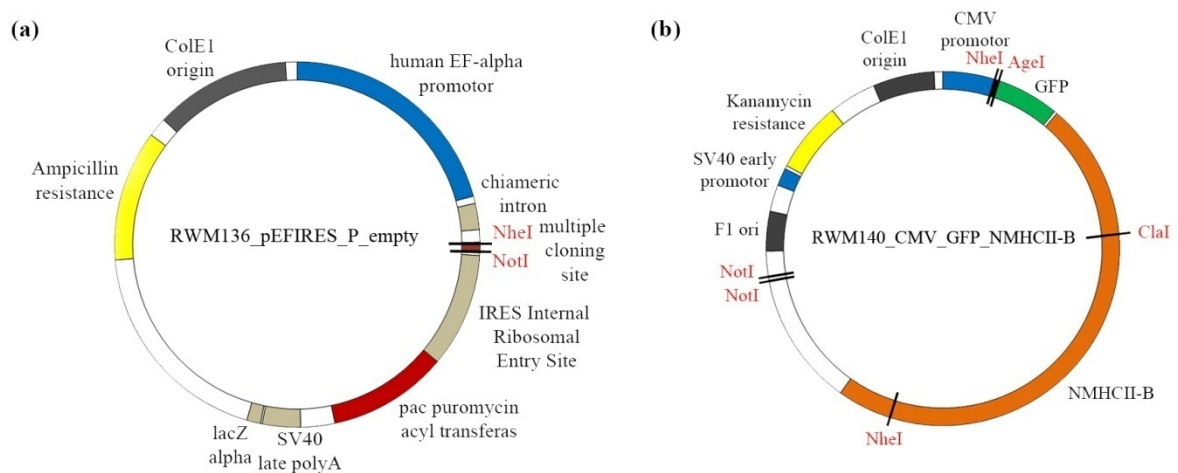


Figure 4: Restriction map of RWM136 and RWM140. (a) The backbone sequence with NheI and NotI cutting sites within the multiple cloning site (MCS). Ampicillin and puromycin resistances are important for a selection in bacteria and mammalian cells. (b) NMHCII-B sequence within the RWM140 construct, flanked with NheI and NotI cutting sites. One additional internal NheI cutting site of the insert sequence requires a three fragment ligation procedure.

Using the restriction enzymes NheI-HF and NotI, the backbone vector was opened at the multiple cloning site (MCS). The insert sequence GFP-NMHCII-B within RWM140 was as well flanked with a cutting site for NheI and NotI respectively. However, the NMHC-II B exhibited a second NheI cutting site inside the insert sequence (Fig. 4b). Considering the large insert length of about 6000 bp, we were not able to obtain a set of enzymes, which cut out the insert without additional cutting sites within the NMHCII-B sequence. Moreover, NheI-HF

and NotI was the only possible combination cutting inside the MCS of the backbone. Therefore a three fragment ligation was the only workable solution as a cloning strategy.

The first insert fragment (insert 1), including the GFP sequence and a part of the NMHCII-B sequence, was produced by cutting the RWM140 construct with NheI-HF and ClaI. Isolating the second section (insert 2) of the myosin sequence the restriction enzymes ClaI and NotI were utilized. However, both ClaI-NotI plasmid fragments were of similar length. Using a third restriction enzyme, AgeI, the unused fragment was additionally cut to run lower in the agarose gel.

The successive table lists the digestion for this cloning procedure.

Table 16: Digest preparation for RWM140 and RWM136.

Insert 1	Insert 2	Backbone
5 µl DNA	5 µl DNA	3 µl DNA
5 µl 10x BSA	5 µl 10x BSA	3 µl 10x BSA
5 µl NEbuffer 4	5 µl NEbuffer 4	3 µl NEbuffer 4
2 µl NheI-HF	2 µl AgeI	0,5 µl NheI-HF
2 µl ClaI	2 µl ClaI	0,5 µl NotI
	2 µl NotI	
31 µl ddH ₂ O	29 µl ddH ₂ O	20 µl ddH ₂ O
50 µl total	50 µl total	30 µl total

As the first cloning strategy seems to be not very effective, an alternative two fragment ligation was conceived, establishing **NMHCII-B_GFP_Hyg**. Therefore two plasmid constructs from the library were used: the RWM65_pAcGFP1-Hyg-Cm_empty construct serving as the backbone and the RWM140_CMV-GFP-NMHCII-B plasmid for isolating the myosin sequence. Utilizing another backbone as before, the antibiotic resistance was changed to hygromycin, a weaker selection marker than puromycin. Moreover, it was possible this time, to take advantage of a two fragment ligation, using a different set of enzymes AgeI and NotI (see Fig. 5).

Cutting with restriction enzymes AgeI and NotI, the backbone vector was opened by isolating the GFP sequence and a part of the MCS. Furthermore, NMHCII-B within RWM140 was flanked with AgeI and NotI cutting sites respectively, including the GFP sequence. Additionally a third restriction enzyme, NdeI, was used, producing a clearly differentiated band pattern in the agarose gel.

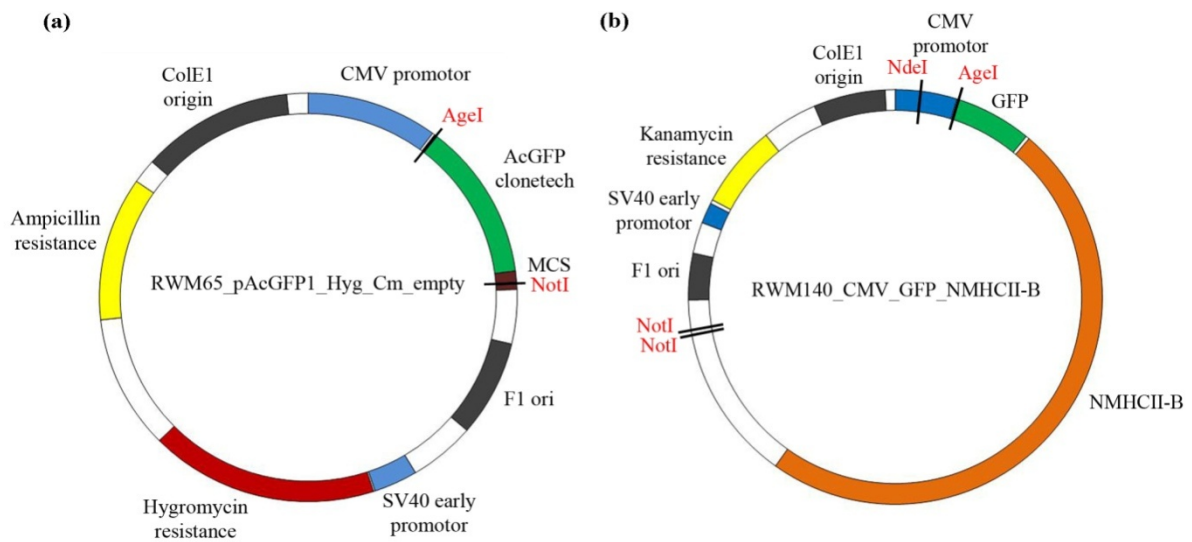


Figure 5: Restriction map of RWM65 and RWM140. (a) The backbone plasmid with AgeI and NotI cutting sites. AgeI is located inside the linker between CMV promoter and GFP sequence and NotI is located within the MCS. Ampicillin and hygromycin resistance are important for a selection in bacteria and mammalian cells. (b) NMHCII-B sequence included in the RWM140 construct, flanked with AgeI and NotI cutting sites.

Cutting with restriction enzymes AgeI and NotI, the backbone vector was opened by isolating the GFP sequence and a part of the MCS. Furthermore, NMHCII-B within RWM140 was flanked with AgeI and NotI cutting sites respectively, including the GFP sequence. Additionally a third restriction enzyme, NdeI, was used, producing a clearly differentiated band pattern in the agarose gel.

Table 17 shows the reaction mixture for producing the insert and the backbone fragment.

Table 17: Digest preparation for RWM140 and RWM65.

Insert		Backbone	
3 μ l	DNA	3 μ l	DNA
3 μ l	10x BSA	3 μ l	10x BSA
3 μ l	NEbuffer 4	3 μ l	NEbuffer 4
0,5 μ l	AgeI-HF	0,5 μ l	AgeI-HF
0,5 μ l	NotI-HF	0,5 μ l	NotI-HF
0,5 μ l	NdeI		
19,5 μ l	ddH ₂ O	20 μ l	ddH ₂ O
30 μ l	total	30 μ l	total

The expected fragment sizes for both cloning strategies are listed in table 18.

Table 18: Expected sequence lengths of DNA fragments after cloning procedure for pEFIRES_eGFP_NMHCII-B_puro and NMHCII-B_GFP_Hyg.

pEFIRES_eGFP_NMHCII-B_puro		NMHCII-B_GFP_Hyg	
fragment	length [bp]	insert	length [bp]
insert 1	2296	insert	8184
insert 2	5897	backbone	5015
backbone	5644	-	-

The two successive figures indicate the DNA fragments with its expected lengths (table 18) after cutting plasmid construct RWM136_pEFIRES_P_empty with NheI-HF and NotI and RWM140_CMV-GFP_NMHCII-B with NheI-HF and ClaI and accordingly with AgeI, ClaI and NotI to establish **pEFIRES_eGFP_NMHCII-B_puro**.

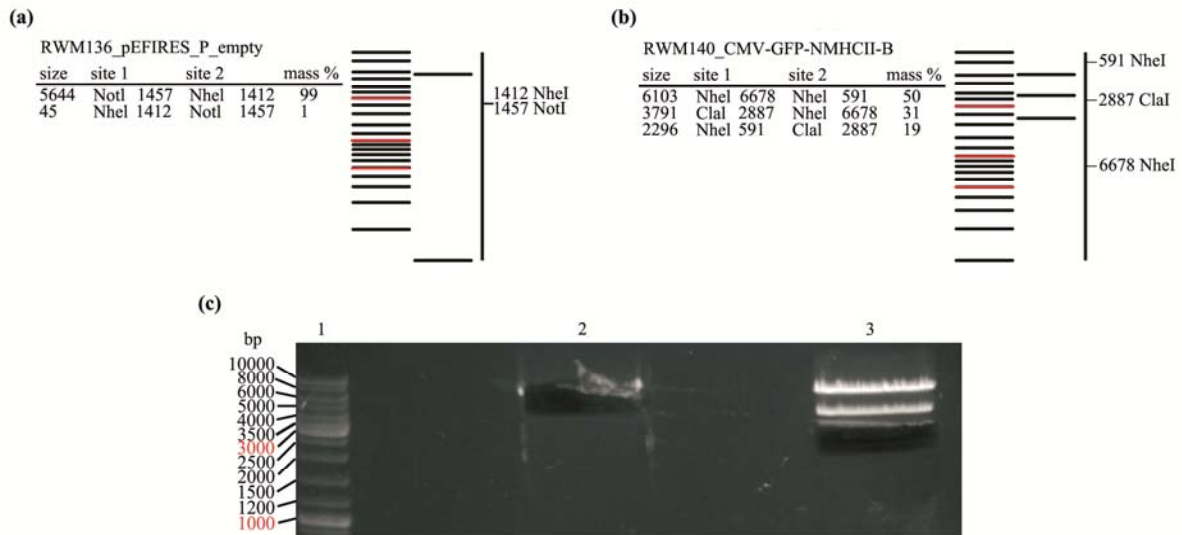


Figure 6: Digest of RWM136 and RWM140 for cloning procedure. This illustration shows the expected band pattern in an agarose gel after cutting **(a)** the backbone with NheI-HF and NotI and **(b)** the insert plasmid with NheI-HF and ClaI. **(c)** 1% TBE agarose gel of insert 1 and backbone. The aliquots were filled up as follows: lane 1, marker (GeneRuler™ DNA Ladder Mix); lane 2, backbone; lane 3, insert 1. The black holes are cut bands for subsequent gel extraction.



Figure 7: Digest of RWM140 for cloning procedure. **(a)** Expected band pattern of RWM140, using ClaI, NotI and AgeI as restriction enzymes. **(b)** 0,8% TBE agarose gel of insert 2. The aliquots were filled up as follows: lane 1, marker (GeneRuler™ DNA Ladder Mix); lane 2, insert 2. The black hole is a cut band for subsequent gel extraction.

Generally the two agarose gels demonstrate a successful digest of RWM136 and RWM140, as all lanes show the expected band pattern. The band of the opened backbone (Fig. 6c, lane 2) can be identified, as expected, near 5500 bp. The double digest for isolating insert 1 (Fig. 6c, lane 3) reveals the band of the NMHCII-B sequence at a length of 2500 bp. Furthermore, the band of insert 2 (Fig. 7b, lane 2) is located at about 6000 bp.

For producing **NMHCII-B_GFP_Hyg** construct, an isolation of the expected DNA fragments succeeded by cutting RWM65 with AgeI and NotI and RWM140 with AgeI, NdeI and NotI. As this elution procedure is analogous to puromycin construct synthesis, it will be not shown in detail.

3.1.2 Ligation procedure

Using the enzyme T4 DNA ligase, the digested DNA fragments were ligated as follows.

Table 19: Reaction mixture for ligation procedure, producing pEFIRES_eGFP_NMHCII-B_puro and NMHCII-B_GFP_Hyg. The DNA fragments were added in two different rates of amount, respectively for both constructs.

pEFIRES_eGFP_NMHCII-B_puro			NMHCII-B_GFP_Hyg	
insert 1	insert 2	backbone	insert	backbone
3	3	1	1	1
36 µg	96 µg	30 µg	48 µg	30 µg
3 µl	4 µl	0,5 µl	8 µl	2 µl
3	1	1	1	2
36 µg	32 µg	30 µg	48 µg	60 µg
3 µl	12 µl	0,5 µl	8 µl	4 µl
			1 µl	T4 DNA ligase
			2 µl	T4 buffer
1,5 µl ddH ₂ O			9,5 µl ddH ₂ O	
20 µl total				

3.1.3 Restriction digests

As a first approach we cut the new construct **pEFIRES_eGFP_NMHCII-B_puro** using restriction enzyme EagI-HF. The following figure presents the results of the first conducted restriction digest (Fig. 8).

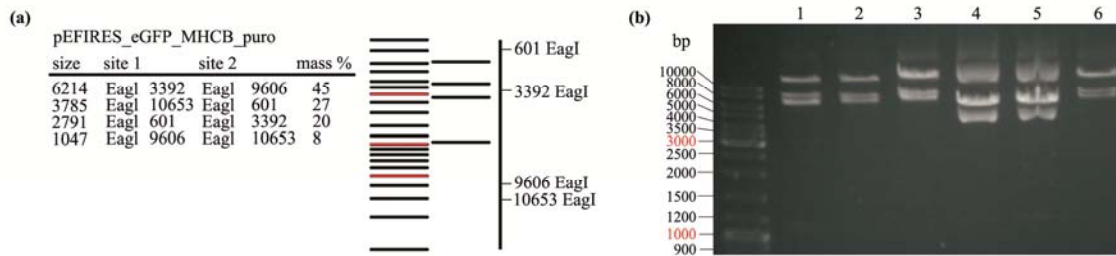


Figure 8: Restriction digest of the new construct pEFIRES_eGFP_NMHCII-B_puro, using EagI-HF.

(a) Chart depicts the expected band pattern after treating the new construct with EagI-HF. (b) 1% TBE agarose gel of the restriction digest. The aliquots were filled up as follows: lane 1, marker (GeneRuler™ DNA Ladder Mix); lane 2 – 7, DNA samples 1 – 6 of six different picked colonies.

Firstly, it can be noticed that all bands appear at a bigger size in comparison to their expected pattern, partly even bigger than 10000 bp. However, examining the band pattern in detail, lanes 2 - 4 and 7 show similarities to the expected pattern. Even the smallest fragment at 1047 bp can be identified as a weak band in the agarose gel. Lane 5 and 6 are presumably uncut with the typical three band pattern related to relaxed, linear and supercoiled uncut plasmid.

Due to the ambiguous results, we performed a second restriction digest (Fig. 9). The samples 1, 2, 4 and 5 were cut with EagI-HF again and compared to EagI-HF cut backbone RWM136 as well as to the uncut version of the new construct. In addition, the samples were cut with NheI-HF and ClaI, two of the restriction enzymes, which were used for the cloning procedure.

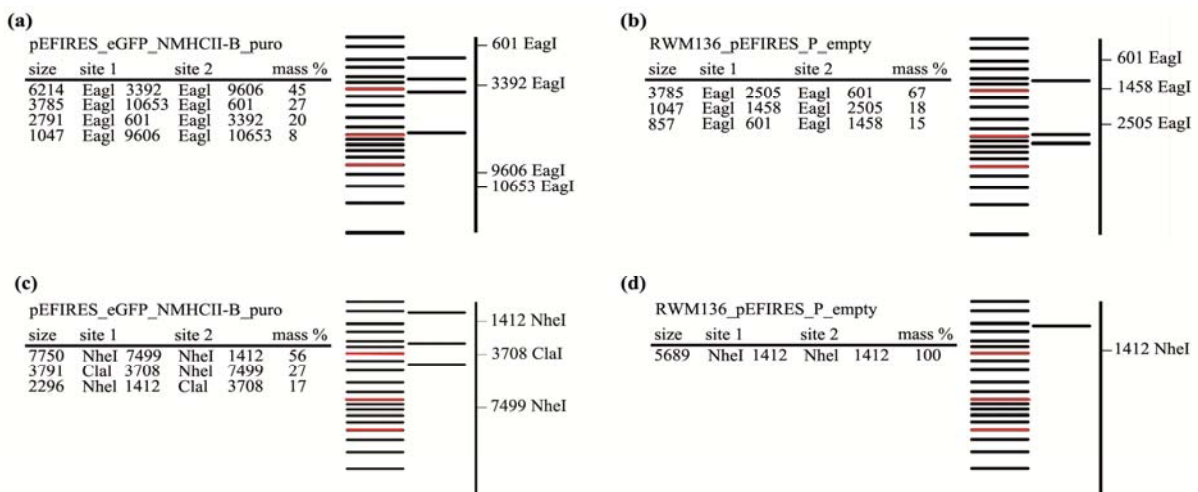


Figure 9.1: Restriction digest of the new construct and the backbone RWM136. Expected band pattern of (a) the new construct when cutting with EagI-HF, (b) the backbone RWM136 when cutting with EagI-HF, (c) the new construct when cutting with NheI-HF and ClaI and (d) the backbone when cutting with NheI-HF.

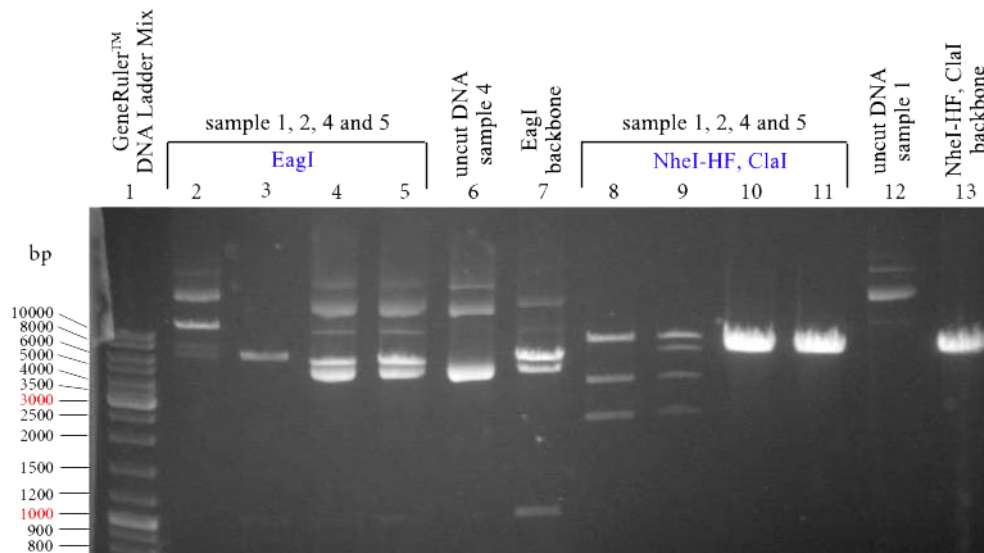


Figure 9.2: 1% TBE agarose gel.

As before, the restriction digest for the EagI-HF cut constructs appears at a bigger size than expected (Fig. 9.2, lane 2 – 5 & 7). Owing to this fact and to the subsequent analysis of NheI-HF-ClaI cut constructs, we assumed the restriction enzyme EagI-HF to be non-functional presumably due to the age of the enzyme. Looking at the double digest of NheI-HF and ClaI, the DNA samples 4 and 5 (Fig. 9.2, lane 10, 11) show the same pattern as the backbone RWM136 (Fig. 9.2, lane 13). The same behavior can be noticed for lane 4 and 5 compared to lane 7. For DNA sample 2, a fourth band appears, which should not exist. We concluded that sample 4 and 5 are backbone plasmids rather than successfully cloned new constructs. These DNA samples were therefore discarded. When comparing to the expected pattern (Fig. 9.1c), only sample 1 (Fig. 9.2, lane 8) resulted in a comparable restriction digest. This sample was therefore further analyzed.

Lastly, the uncut version of the plasmid DNA 1 (Fig. 9.2, lane 12) again illustrates the typical band pattern of circular DNA: relaxed, linear and supercoiled plasmid. The uncut DNA sample 4 seems not to have such typical structures.

The obtained agarose gel in figure 9.2 prompted us to crosscheck only sample 1 again, using various enzymes for restriction digests (Fig. 10). Moreover, the initial plasmids RWM136 and RWM140 were included in the analysis.

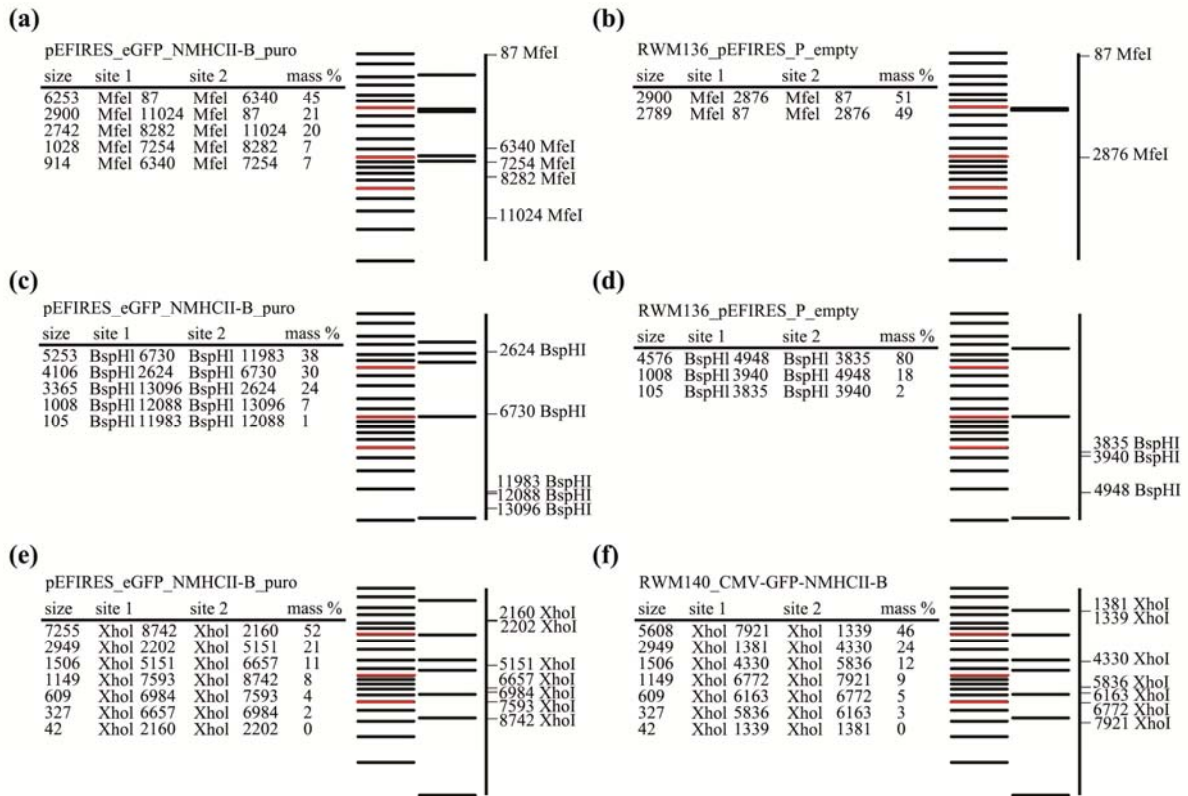


Figure 10.1: Restriction digest of the new construct, RWM136 and RWM140. Expected band pattern of (a) the new construct when cutting with MfeI-HF, (b) the backbone when cutting with MfeI-HF, (c) the new construct when cutting with BspHI, (d) the backbone when cutting with BspHI, (e) the new construct when cutting with XhoI and (f) the insert plasmid when cutting with XhoI.

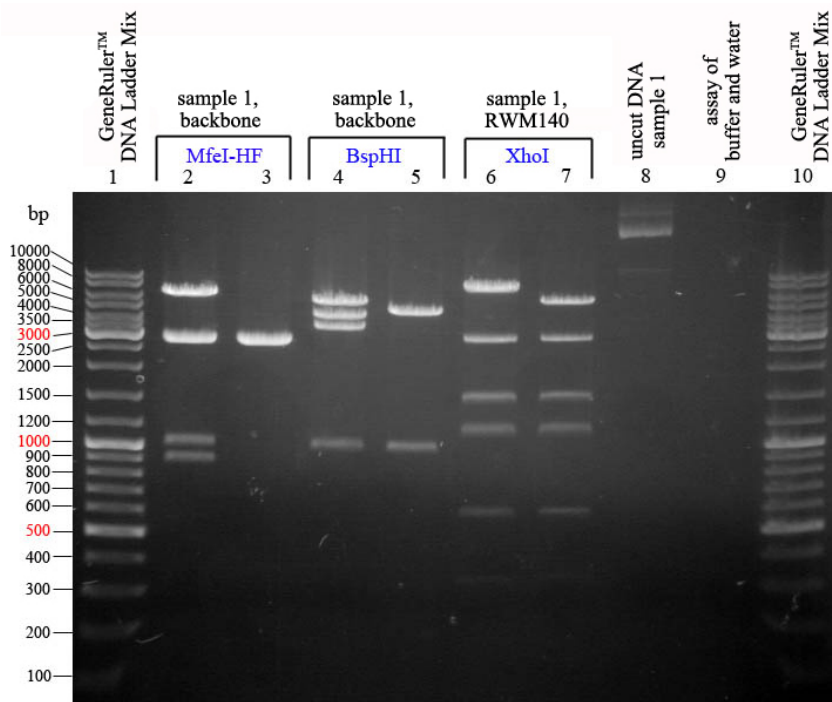


Figure 10.2: Restriction digest of the new construct, RWM136 and RWM140. 1% TBE agarose gel.

In general, cutting DNA sample 1 with MfeI-HF (Fig. 10.2, lane 2), BspHI (Fig. 10.2, lane 4) and XhoI (Fig. 10.2, lane 6), all lanes show expected band sizes. Furthermore, we compared the digests to same cuts of the initial backbone plasmid RWM136 (Fig. 10.2, lanes 3, 5) and RWM140 (Fig. 10.2, lane 7) to verify identifiable differences or similarities. According to Fig. 10.1 the backbone and the insert plasmid also present the expected band patterns. In lane 8 (Fig. 10.2) the uncut version of DNA sample 1 shows again the typical forms of relaxed, linear and supercoiled plasmid.

Producing additional DNA samples of pEFIRES_eGFP_NMHCII-B_puro, we conducted the same cloning strategy once more, using XhoI as enzyme for three new plasmid samples (Fig. 11). Furthermore, there was RWM140, the uncut DNA plasmid and the backbone RWM136 tested, again. Looking at the agarose gel (Fig. 11b) all samples show, according to the expected band pattern (Fig. 10.1 and 11a), a positive outcome.

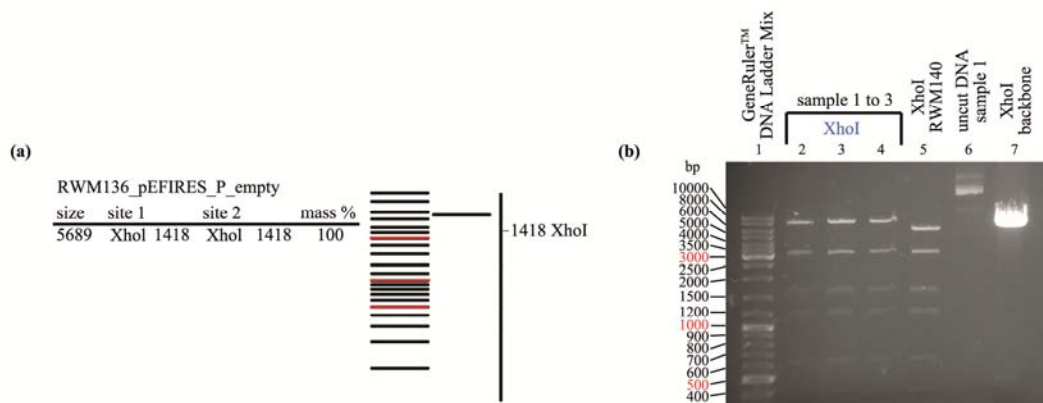


Figure 11: Restriction digest of pEFIRES_eGFP_NMHCII-B_puro, RWM140 and RWM136. (a) Expected band pattern of the backbone when cutting with XhoI and (b) 1% TBE agarose gel

In Fig. 12.2 the results of the new construct NMHCII-B_GFP_Hyg are given as a restriction digest. Therefore six plasmid samples from different picked colonies were cut, using EcoRI as restriction enzyme. Additionally, an EcoRI cut RWM65 construct, an EcoRI and AgeI cut RWM140 construct and the uncut version of the new construct were examined for comparison.

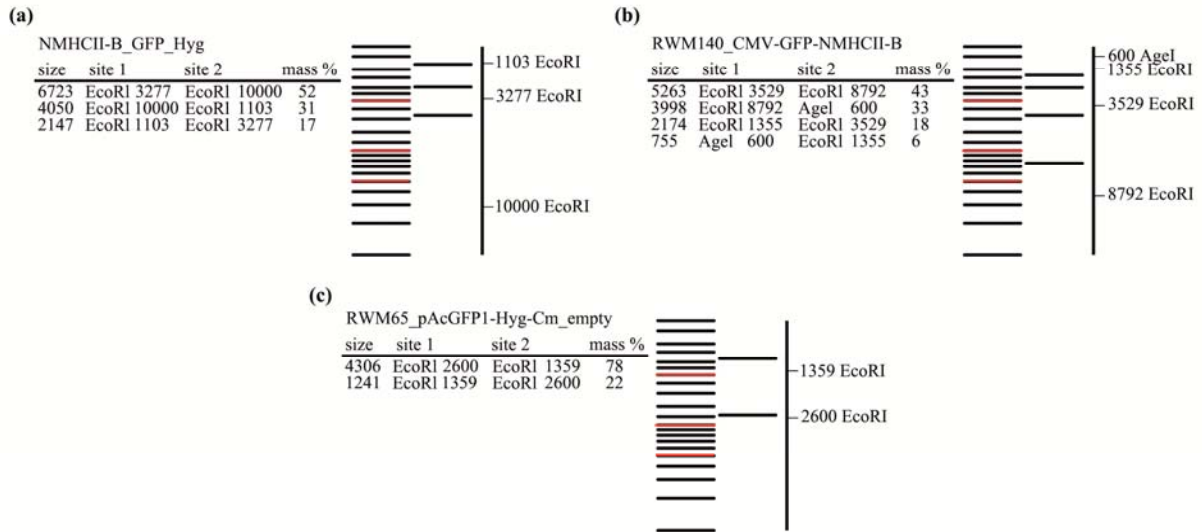


Figure 12.1: Restriction digest of the new construct NMHCII-B_GFP_Hyg, RWM140 and RWM65. Expected band pattern of (a) the new construct, (b) the insert construct RWM140 and (c) the backbone, when cutting with EcoRI.

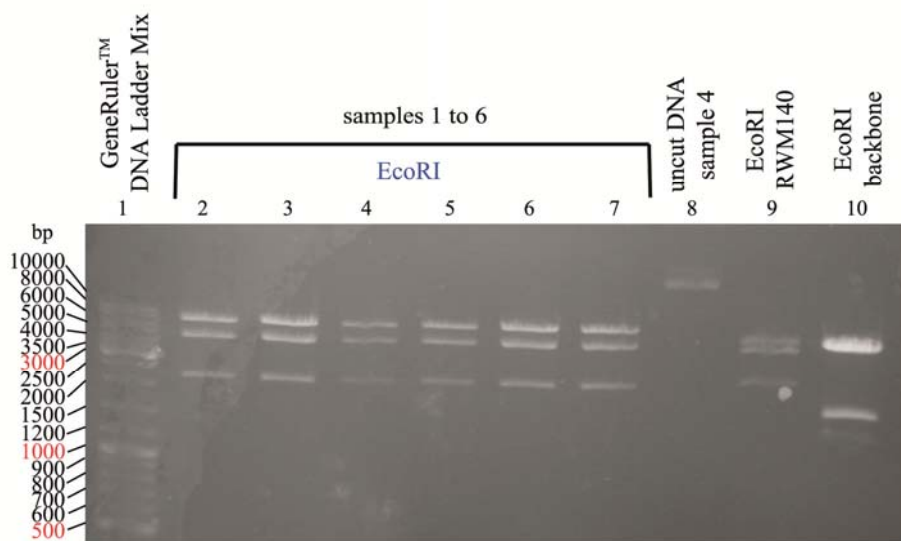


Figure 12.2: Restriction digest of the new construct NMHCII-B_GFP_Hyg, RWM140 and RWM65. 1% TBE agarose gel.

Generally, the restriction digest depicts a successfully proceeded cloning of NMHCII-B_GFP_Hyg, as DNA sample 1 – 6 (Fig. 12.2, lane 2 – 7) show the expected band pattern. The uncut plasmid of sample 4 (Fig. 12.2, lane 8) presents again the bands for relaxed, linear and supercoiled DNA. Looking at lane 9 and 10, RWM65 and RWM140 also illustrate the expected band sizes.

3.1.4 Sequencing

To test a correct insertion in the backbone and a successful incorporation of both NMHCII-B insert fragments concerning pEFIRES_eGFP_NMHCII-B_puro sample 1 (Fig. 10.2), we used two different primers 5'-NMHCII-B-2 and 5'-NMHCII-B-10 (table 8). The complementary sequences for the primers are shortly before and after the ClaI cutting site, located within NMHCII-B sequence. The primers synthesized an error free complementary DNA strand of pEFIRES_eGFP_NMHCII-B_puro sample 1.

Moreover, we ordered a second sequencing to check the cutting sites NheI and NotI of the pEFIRES_eGFP_NMHCII-B_puro construct. Sample 1 (Fig. 10.2) of our first approaching digest and sample 1 and 2 (Fig. 11b) of our second approach digest were mixed respectively with two primers 3'EGFP-seq and IRES-3'seq (table 8), for sequencing in reverse direction. The human EF-alpha promotor sequence (see Fig. 4a) within the backbone RWM136 showed high repetitive C-sequences. Due to this, some base positions in these sequence parts could not be identified clearly as shown in Chromas Lite Software. Additionally, two missense mutations appeared inside the promotor sequence. The same behavior could be noticed for pEFIRES_eGFP_NMHCII-B_puro DNA samples 1 and 2 (Fig. 11b) of the second restriction digest.

3.2 Cell culture

After growing of MDCK wildtype cells in 12 well plates, the obtained constructs pEFIRES_eGFP_NMHCII-B_puro and NHMCII-B_GFP_Hyg were used for single and double transfection. NMHCII-B motor protein was once double transfected with NMHCII-A and once with non-muscle myosin regulatory light chain (NMRLC).

However, it was impossible to establish stable cell lines. Adding the respective selection marker after transfection procedures, all transfected MDCK cells died within one week antibiotic treatment.

Due to this problem, we decided to perform transient transfections. Therefore, we additionally applied RWM140_CMV-GFP-NMHCII-B and a Lifeact-GFP construct RWM142_pEGFP-N1-Lifeact-Hyg for transfection control. Using RWM142, we obtained a positive outcome of the transfection procedure by taking advantage of a high expression level of Lifeact-GFP. In comparison, RWM140 cells and cells including the new constructs exposed a significantly lower expression level, 24 h after transfection.

Our first approach was to transfer transfected cells 24 h after transfection procedures in small microscope dishes, to visualize GFP enhanced cells 48 h later. Neither RWM140 transfected cells, nor pEFIRES_eGFP_NMHCII-B_puro and NHMCII-B_GFP_Hyg transfected MDCK II cells showed any potential fluorescence expression for live cell imaging. We further conducted the same transfections in HeLa cells and received the same results.

As the pEFIRES_eGFP_NMHCII-B_puro construct exhibited two missense mutations within the promotor sequence, we decided to concentrate on RWM140 and NHMCII-B_GFP_Hyg for subsequent imaging.

Furthermore, we changed the time difference between transfection and transfer procedure in a second run through, to investigate the variance of fluorescence levels:

- Directly after transfection
- 12 h after transfection
- 24 h after transfection

Generally the expression level decreases from 0 to 24 h rapidly for both constructs respectively. Due to this behavior live cell imaging was mainly possible directly and 12 h after transfection procedure. Certainly, most cells showed overexpression and no good morphology.

As our last approach, we transfected RWM140 and NHMCII-B_GFP_Hyg plasmids directly in microscope dishes to diminish a fluorescence loss. MDCK II cells with the geneticin as well as cells with the hygromycin construct showed a good expression level for live cell imaging.

For double transfection procedures we focused on transfecting in microscope dishes respectively for NMHCII-B-NMHCII-A and NMHCII-B-NMRLC. Due to a laser breakdown at that point of time, there was no live cell imaging possible. Only receptions from the bottom of the cells were generated.

3.3 Characterization

3.3.1 Structure of NMHCII-B

In comparison to NMHCII-A, isoform B showed the same characteristic structures in non-confluent cells (Fig. 13). Visualizing the apical side and the midsection of NMHCII-B transfected epithelial MDCK II cells, an isotropic cortical network could be identified

(Fig. 13a,c). The basal side of the cells revealed stress-fibers, actin dependent structures linking through wired integrins to the cell substrate [2]. Integrins are heterodimeric transmembrane proteins, functioning as connection between extracellular matrix and actomyosin cytoskeleton [1,2]. Additionally, accumulated actomyosin structures were depicted at the free cell edge near the basal membrane (see red arrows in Fig. 13e).

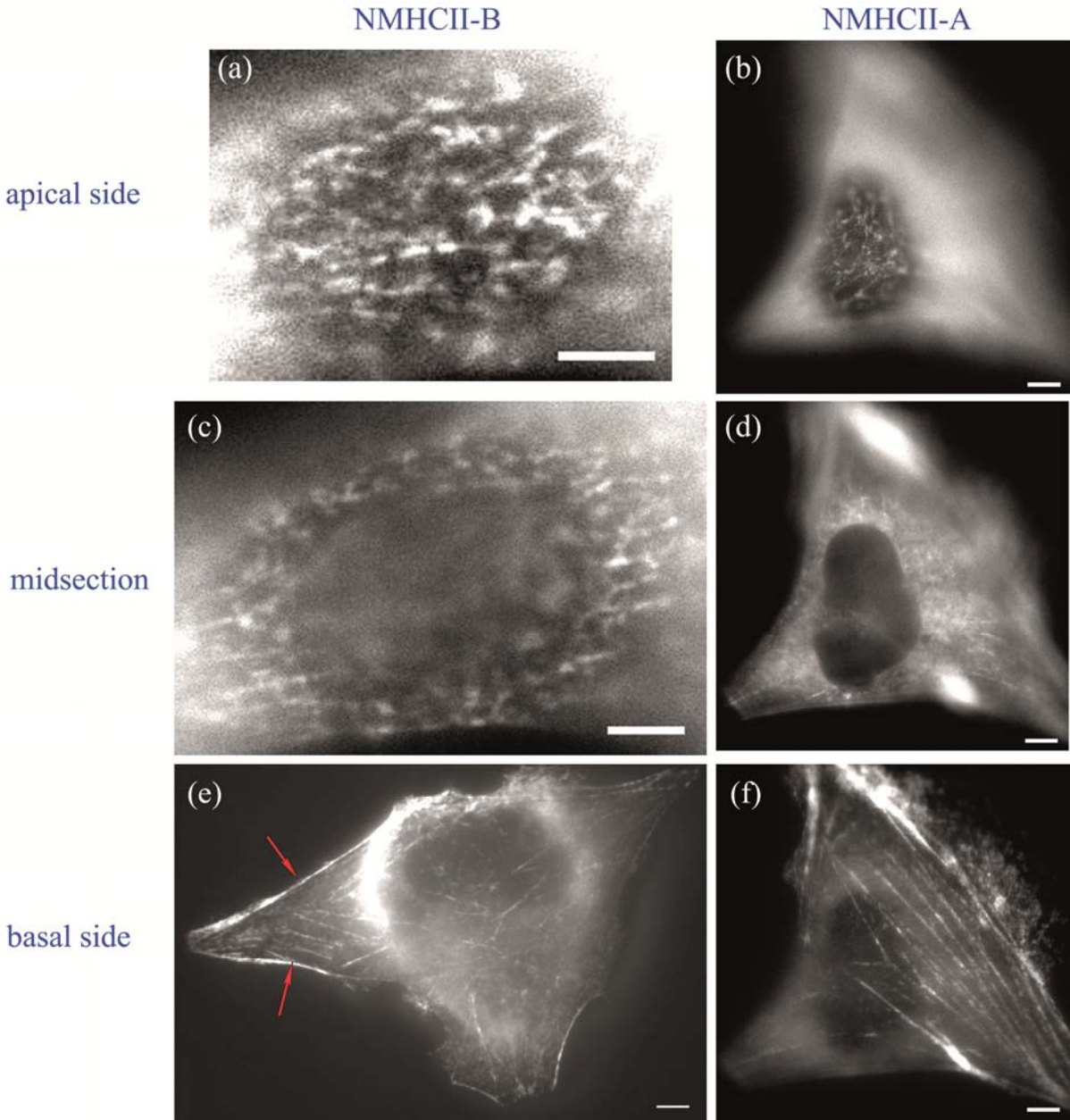


Figure 13: Structure of NMHCII-B in non-confluent epithelial cells in comparison to NMHCII-A. (a), (b) Isotropic network at apical side, scale bar: 3 μm (a) and 5 μm (b). (c), (d) Isotropic network at midsection, scale bar: 3 μm (c) and 5 μm (d). (e), (f) Stress-fibers at the basal side, scale bar: 3 μm (e) and 5 μm (f).

Furthermore, a second structural accordance to NMHCII-A was a dome-shaped arrangement of the myosin network (Fig. 14), spanned over the whole non-confluent apical cell cortex. In Fig. 14 b,c shown results are unpublished data obtained by Christoph Klingner.

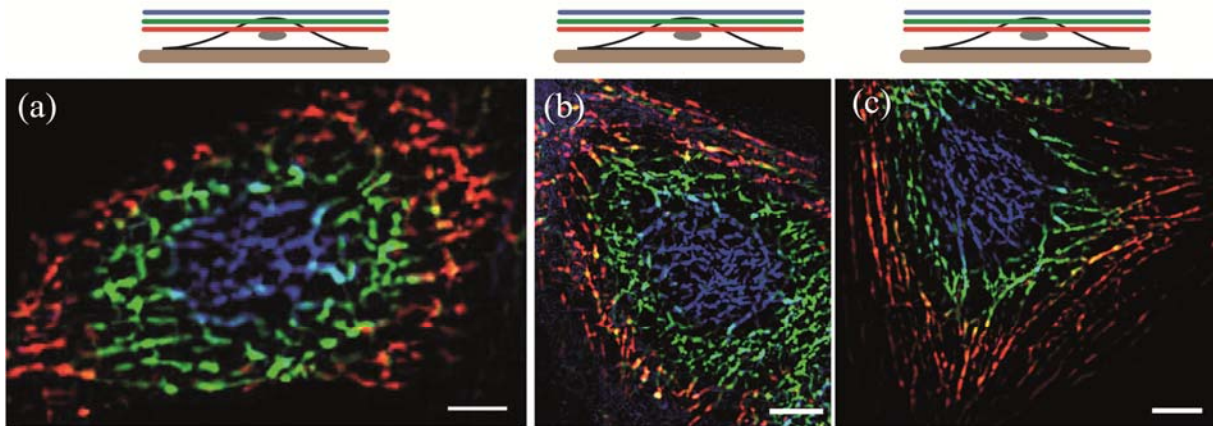


Figure 14: Structural arrangement of myosin II at the apical side of MDCK cells. Dome-shaped structure of (a) NMHCII-B, scale bar: 3 μm , (b) NMHCII-A, scale bar: 5 μm and (c) NMRLC, scale bar: 5 μm ; (b) and (c) data by C. Klingner.

Looking at confluent MDCK cells, GFP labeled non-muscle myosin heavy chain II B depicted dot-like structures at the surface (Fig. 15a). This behavior was observable for NMHCII-A as well, resembling unpublished data obtained by Christoph Klingner.

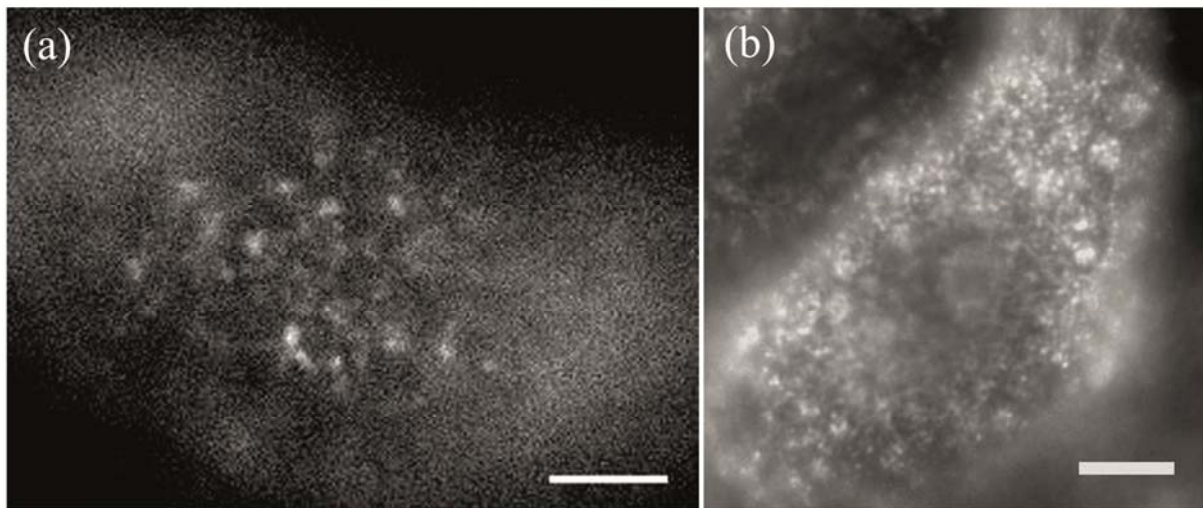


Figure 15: Structure of myosin II in confluent epithelial cells at the apical side. Dot-like structure of (a) NMHCII-B and (b) NMHCII-A. Scale bar: 5 μm ; (b) data by C. Klingner.

A double transfection of NMHCII-B and NMRLC, led only to images showing the bottom of MDCK cells. In both cases, for GFP labeled heavy chain and for mCherry labeled light chain, a distinctive stress-fibers network existed. By overlaying the green and the red color, a yellow image followed as both proteins showed identical stress-fibers patterns (Fig. 16).

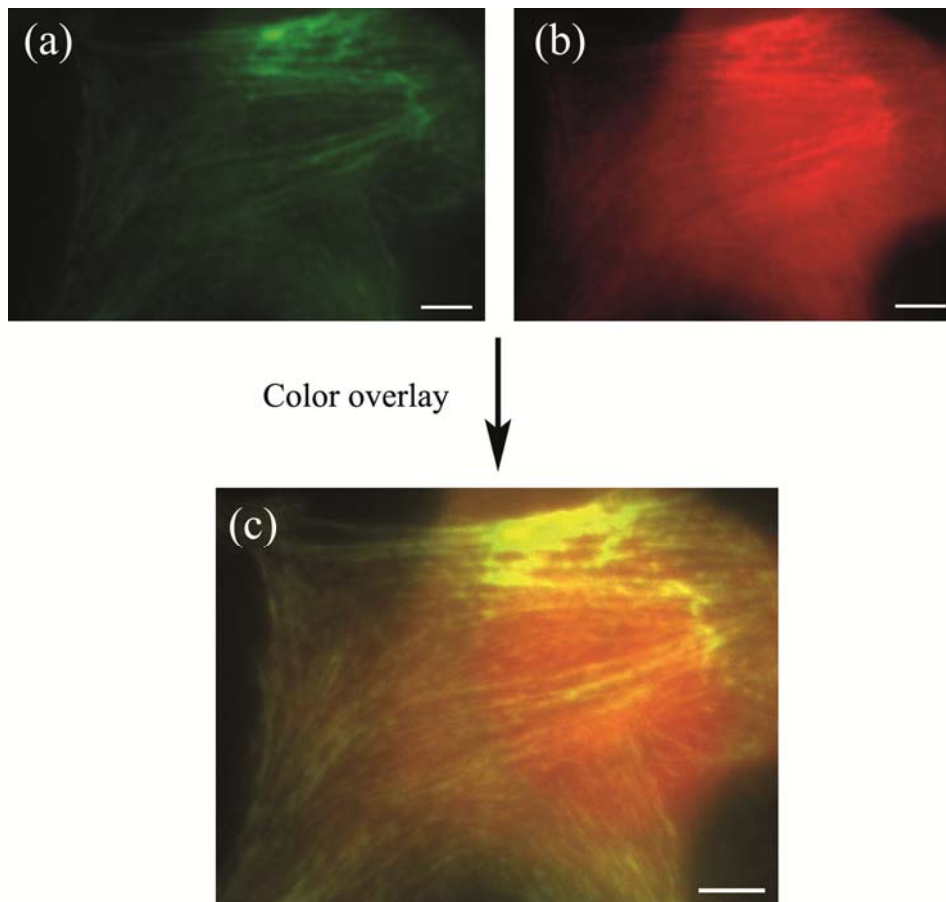


Figure 16: Images of MDCK II cell after double transfection of NMHCII-B (green) and NMRLC (red). (a) GFP labeled stress-fibers of myosin heavy chain, (b) mCherry labeled stress-fibers of myosin light chain, (c) color overlay of NMHCII-B and NMRLC. Scale bar: 5 μm .

3.3.2 Dynamical behavior

The kymograph in Fig. 17 illustrates a correlated motion pattern on 3 μm distance of NMHCII-B motor proteins within the isotropic cortical network. Identifying parallel stripes, contiguous myosin II B structures showed dependent movement. Further distant structures on the contrary exhibited different moving behavior, as the kymograph features, varying stripe structures.

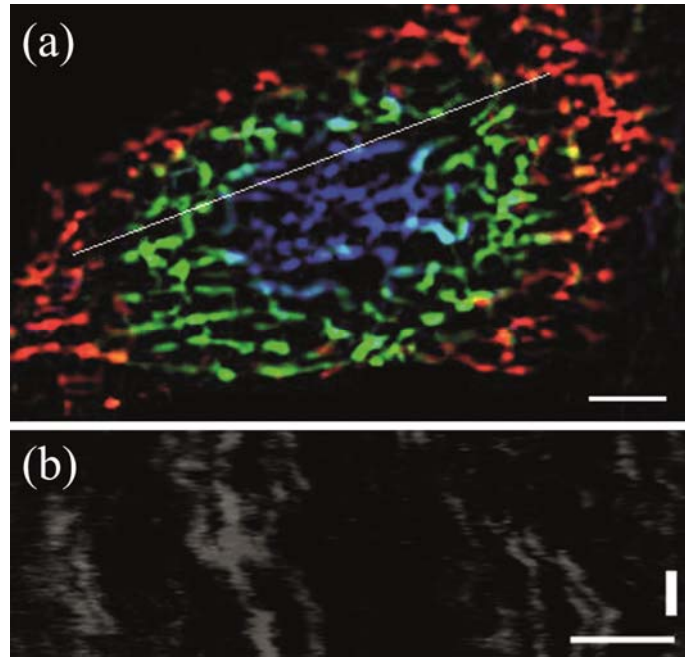


Figure 17: Structural and dynamical arrangement at the apical side of MDCK cells. (a) dome-shaped structure as color-overlay illustration, scale bar: 3 μm . **(b)** kymograph, scale bar: 3 μm , 100 sec.

The graph in Fig. 18 highlights the temporal autocorrelation by Pearson, as the Pearson correlation coefficient r is plotted against time t . Correlation coefficient r demonstrates a rapid decrease from 1,0 to 0,3 within 100 seconds for all ($N = 23$) specified filtered data of time-lapse movies of NMHCII-B transfected MDCK II cells. After 100 seconds, the curve generally flattens and the amounts for r level off between 0,3 and 0,2. Three exemplary correlation coefficients and their respective exponential fits are shown.

The obtained correlation spectroscopy data was fitted using Origin[®] Pro 9.0 and the following fitting function:

$$r = r_0 + Ae^{-x/\tau}$$

r: Pearson correlation coefficient, r_0 : offset, A: intercept, x: time, τ : decorrelation time

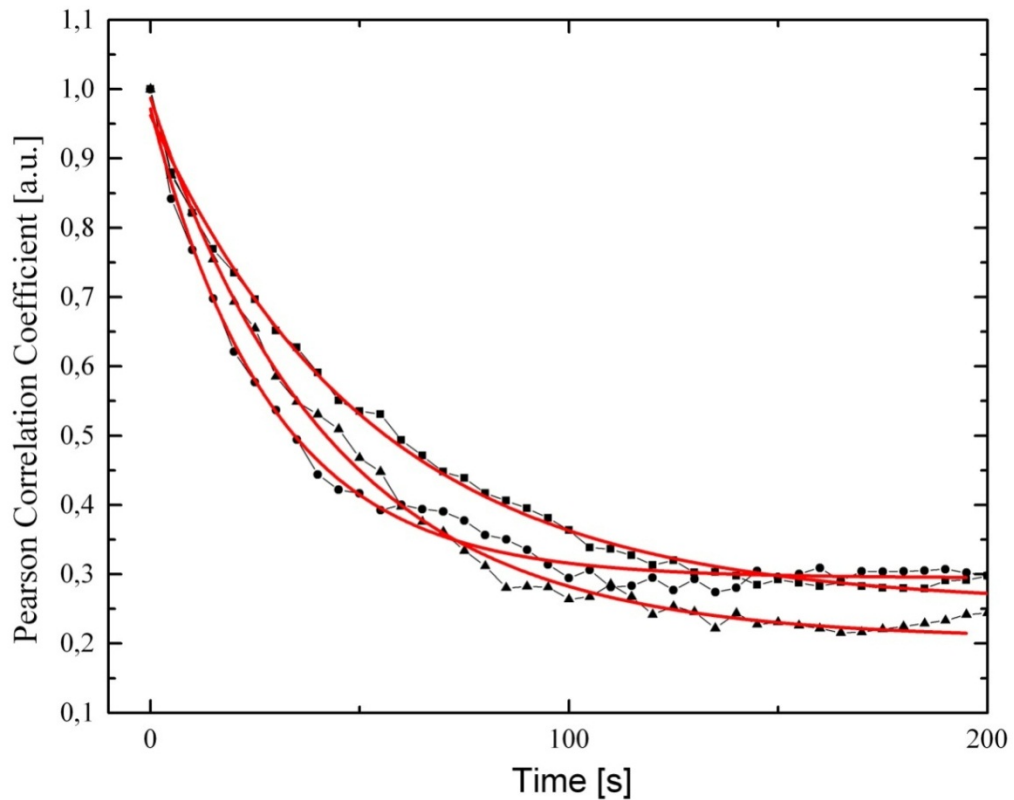


Figure 18: Temporal autocorrelation spectroscopy and exemplary fitting curves.

The amounts with respective error for decorrelation time τ of $N = 23$ mammalian cells are listed in table 20. A recognizable fluctuation of τ from 59 ± 7 sec as the highest to 22 ± 1 sec as the lowest, leads to an resulting average of 39 ± 3 sec.

Table 20: Decorrelation time $\tau(\pm \text{SE})$ of NMHCII-B_GFP_Hyg and RWM140 transfected cells.

cell	decorrelation time τ [sec]	cell	decorrelation time τ [sec]
NMHCII-B_GFP_Hyg transfected cells		RWM140_CMV-GFP-NMHCII-B transfected cells	
1	24 ± 2	11	36 ± 1
2	58 ± 2	12	28 ± 1
3	51 ± 2	13	44 ± 2
4	59 ± 7	14	53 ± 4
5	33 ± 1	15	35 ± 1
6	43 ± 2	16	36 ± 1
7	29 ± 2	17	33 ± 2
RWM140_CMV-GFP-NMHCII-B transfected cells		18	53 ± 2
8	39 ± 2	19	46 ± 5
9	22 ± 1	20	29 ± 1
10	35 ± 2	21	33 ± 3
		22	43 ± 1
		23	23 ± 1

In comparison to NMHCII-A and NMRLC the average timescale for NMHCII-B is lower (table 21). Using the Standard-Error SE, a histogram (Fig. 19) shows the time differences within the movement behavior of these three motor proteins in non-confluent cells. The data for NMHCII-A and NMRLC was obtained by Christoph Klingner.

Table 21: Average timescale (\pm SE) of NMHCII-B, NMHCII-A and NMRLC and respective cell number.

	NMHCII-B	NMHCII-A	NMRLC
timescale $\tau \pm$ SE [sec]	39 ± 11	60 ± 10	58 ± 9
cell number	N = 23	N = 14	N = 9

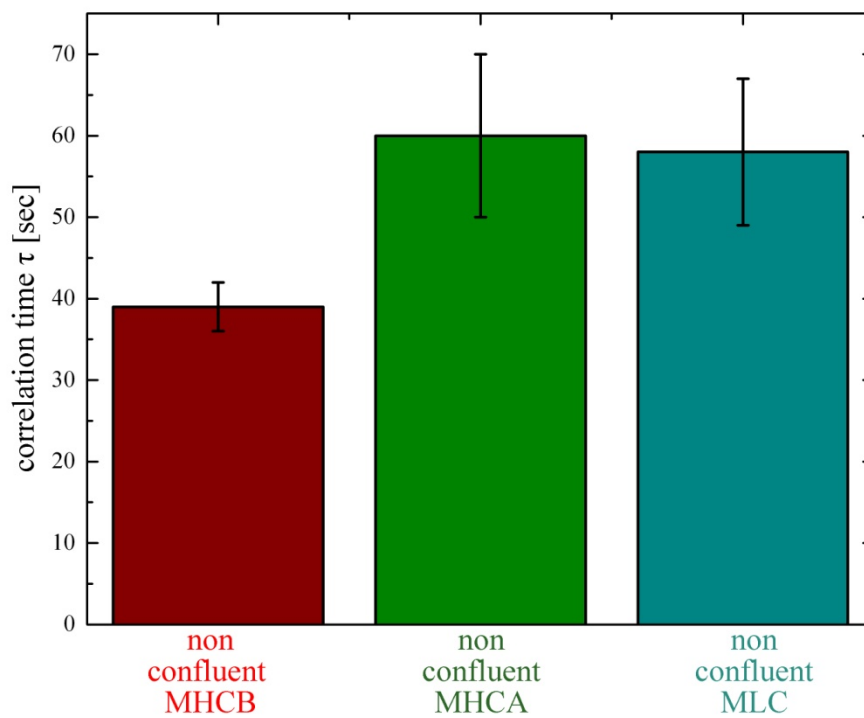


Figure 19: Average correlation time τ of non-confluent MHC B, MHC A and MLC.

Furthermore, myosin-II-B contributes to oscillatory behavior (Fig. 20), looking at a trend of correlation time τ over time t of one single time-lapse movie. The maxima stand for slow and the minima for fast movement of NMHCII-B motor proteins. At about $\tau = 47$ sec the curve reaches its highest level. This correlation time corresponds almost to the obtained data of MHCA and MLC (Fig. 18). The minima describing fastest reorganization is reached at $\tau = 18$ sec. Concerning a photo-bleaching effect within live cell imaging, no clearly statement could be made after time $t = 250$ sec anymore.

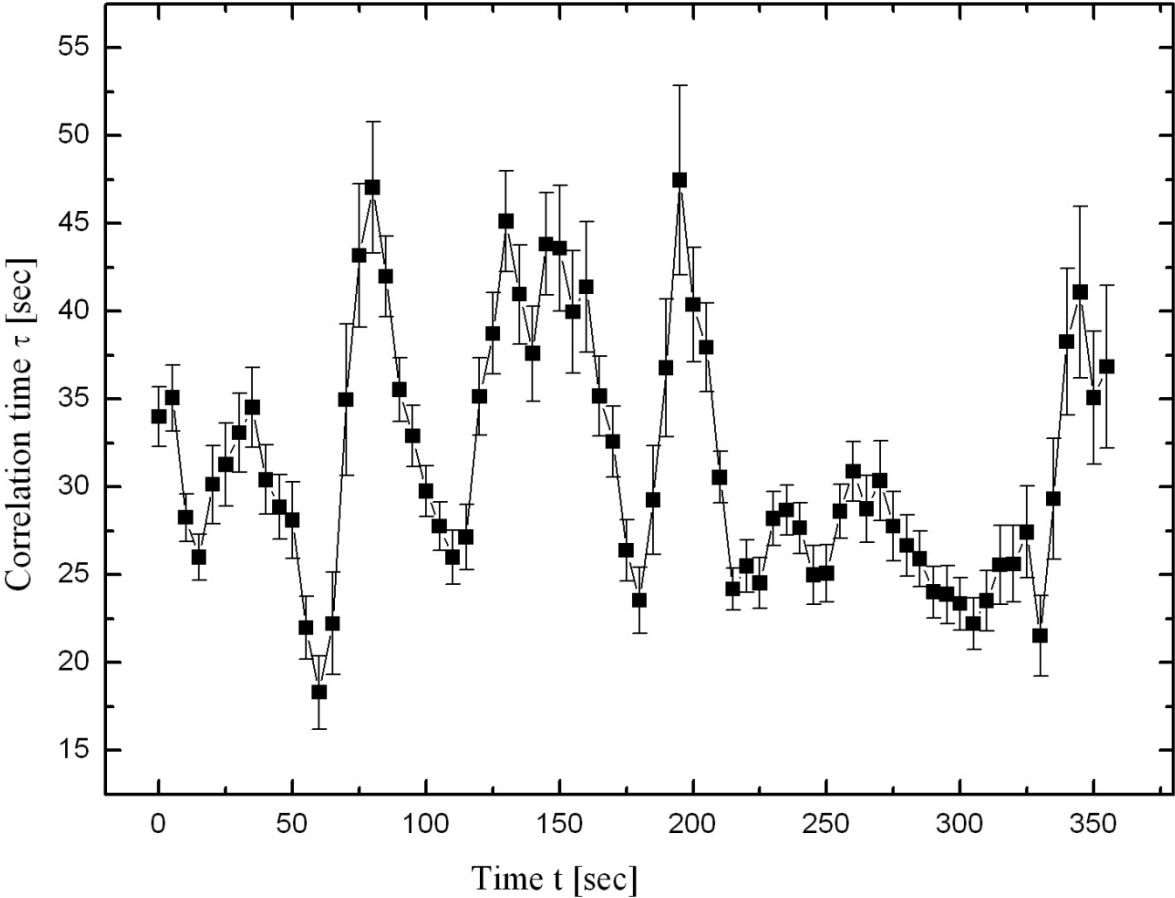


Figure 20: Oscillatory behavior of NMHCII-B motor proteins.

4 Discussion

4.1 Molecular Biology

The results of the cloning strategies of the new constructs pEFIRES_eGFP_NMHCII-B_puro and NMHCII-B_GFP_Hyg show a positive outcome, as final restriction digests (see Fig. 10.2, 11, 12.2) correspond to expected band patterns. We therefore concluded both plasmid constructs to be correctly generated. However, checking the cutting sites by sequencing methods the promoter sequence shows dependent on its high repetitive C-sequences two missense mutations, respectively for pEFIRES_eGFP_NMHCII-B_puro constructs. Due to this aspect, a low expression level of myosin II-B in MDCK II cells can be expected. Nevertheless, we used both new constructs pEFIRES_eGFP_NMHCII-B_puro and NMHCII-B_GFP_Hyg for subsequent transfection procedures.

4.2 Cell culture

After successful cloning procedures, it was impossible to stably express MDCK II cell lines with transfected NMHCII-B plasmid sequences. Considering the fact of the 6000 bp large myosin sequence, included in a 10 000 bp long plasmid, complicates transfection into MDCK II cells. For all conducted transfection procedures, all cells died within one week antibiotic treatment, thereby resulting in no successful transfection of the new constructs. However, using RWM142 (Lifeact-GFP) as control, transfection procedure has been proofed as workable. Additionally, establishing stable cell lines is based on integration of the plasmid sequence within the mammalian genome, which in this case might secondly reach its limits. Whether error-prone plasmids lead to the incapability of stable cell line generation or a transfection procedure modification would result in positive stable clones, remains to be elucidated. To avoid these complications, we conducted transient transfection procedures.

4.3 Live cell imaging

Visualizing the cells, a rapid loss of fluorescence expression within 48 hours takes place. In transient transfections the plasmid constructs remain freely in the cell matrix, MDCK II cells could recognize the new construct as foreign substance and DNases degrade the plasmid. With no further NMHCII-B synthesis, the fluorescence expression decreases as well. To diminish this fluorescence degradation, transfecting directly in microscope dishes emerges as best solution. However, conducting transient transfection most cells show overexpression artifacts and phenotypic effects. The new construct NMHCII-B_GFP_Hyg firstly consists of a strong promotor, increasing protein expression. Secondly, an extrachromosomal myosin II-B

sequence additional to a NMHCII-B sequence within the MDCK II cell genome leads to strongly enhanced protein synthesis. Overexpressed myosin proteins are degraded and packed in vesicles, as seen in Fig. 3 (red dots). Using western blotting techniques for further studies, the expression level of NMHCII-B motor proteins in transfected MDCK II cells could be tested in comparison to MDCK II wildtype cells.

As a result of missense mutations inside the promotor sequence, myosin II-B proteins might be synthesized in low amounts or even not all and will therefore show little or no fluorescence expression. For further investigation, it might be interesting to check the whole NMHCII-B sequence within pEFIRES_eGFP_NMHCII-B_puro and NMHCII-B_GFP_Hyg to eliminate mutations and with it a wrong synthesized myosin II-B protein.

Moreover, the linker sequence within the new constructs, located between GFP and NMHCII-B sequence, exhibits in comparison to NMHCII-A an additional codon, coding for amino acid proline. The effects on GFP labeled myosin II-B motor proteins are on this account not predictable. Preventing a functional inhibition of NMHCII-B due to steric effects as worst case, it will be necessary to test the linker on its behavior or to change the linker sequence with a well-known linker sequence by polymerase chain reaction (PCR) cloning strategy.

The aim of my bachelor thesis was to investigate the localization and dynamics of NMHCII-B in comparison to NMHCII-A obtained data, according to Roland Wedlich-Söldner group.

Like isoform II-A, myosin II-B localizes to the new cortical myosin network at the apical side of non-polarized MDCK II cells (see Fig. 13a,b). Showing similar structures, we hypothesize that both isoforms take part in same cellular functions. Levayer et al [5] pointed out that MHCA and MHCB are recruited in different manner. Moreover, these two proteins differ significantly in dynamics with MHCA being a fast motor while MHCB acts as a potent stabilizing factor [5]. In the course of this study however, it was impossible to establish double transfections to analyze colocalization and protein interplay to confirm these statements. Double transfecting NMHCII-B and NMRLC, we only succeeded in generating images from the basal part of cells where stress-fiber structures colocalize (see Fig. 16c). For further investigations, it will be of high interest to reach convincing results in double transfection procedures.

Comparing the dynamic behavior of NMHCII-B with isoform II-A using correlation spectroscopy, decorrelation time τ is meanly lower (see Fig. 19). Myosin II-B shows therefore faster movement within the cortical actomyosin network of MDCK II epithelial cells. Certainly, conducting transient transfection lead to overexpression artifacts, which negatively influence fluorescence signal and thereby calculations of pearson temporal autocorrelation. Additionally NMHCII-B contributes to oscillatory behavior switching between periods of fast and slow network reorganization, as a quantitative diagram in Fig. 19 proofs. Again, it will be important to generate qualitative data, establishing stable cell lines with transfected myosin II-B.

Taken together, our obtained data of non-muscle myosin II-B shows similarities in localization and dynamics to isoform II-A. Though these similarities already indicate that NMHCII-A and NMHCII-B feature the same cellular functions, the influence of overexpression effects due to transient transfections hinder the generation of significant and comparable data. The establishment of stable cell lines by e.g. modifying the transfection protocol and adapting plasmid constructs is therefore of high interest for further studies on this project.

5 References

- 1 Clark K., Langeslag M., Figdor C.G., van Leeuwen F.N., *Myosin II and mechanotransduction: a balancing act*. Trends Cell Biol., 2007. **17**(4): p. 178-86.
- 2 Vicente-Manzanares M., Ma X., Adelstein R.S., Horwitz A.R., *Non-muscle myosin II takes centre stage in cell adhesion and migration*. Nat Rev Mol Cell Biol., 2009. **10**(11): p. 778-90.
- 3 Watanabe T., Hosoya H., Yonemura S., *Regulation of myosin II dynamics by phosphorylation and dephosphorylation of its light chain in epithelial cells*. Mol Biol Cell., 2007. **18**(2): p. 605-16.
- 4 Beach J.R., Hussey G.S., et al., *Myosin II isoform switching mediates invasiveness after TGF- β -induced epithelial-mesenchymal transition*. Proc Natl Acad Sci U S A, 2011. **108**(44): p. 17991-17996.
- 5 Levayer R., Lecuit T., *Biomechanical regulation of contractility: spatial control and dynamics*. Trends Cell Biol, 2012. **22**(2): p. 61-81.
- 6 Spira F., Mueller N.S., et al., *Patchwork organization of the yeast plasma membrane into numerous coexisting domains*. Nat Cell Biol., 2012. **14**(6): p. 640-648.
- 7 Rodgers J.L., Nicewander W.A., *Thirteen ways to look at the correlation coefficient*. The American Statistician, 1988. **42**(1): p. 59-66.

6 Acknowledgements

I would like to thank all members of the Roland Wedlich-Söldner group for supporting me during my bachelor thesis. It was a great pleasure to work in such a nice and friendly atmosphere.

Especially, I want to thank Dr. Roland Wedlich-Söldner for giving me a chance to work on this project and Christoph Klingner for helping me with experimental